Laser Physics

Astro Ltd.

PAPER

Erbium-doped fiber ring laser with wavelength selective filter based on non-linear photonic crystal fiber Mach–Zehnder interferometer

To cite this article: W A Khaleel and A H Al-Janabi 2017 *Laser Phys.* **27** 105104

View the article online for updates and enhancements.

Related content

- Switchable and tunable erbium-doped fiber lasers using a hollow-core Bragg fiber
Tanglin Zhao, Zhenggang Lian, Xin Wang et al.
- A tunable multi-wavelength laser based on a Mach–Zehnder interferometer with photonic crystal fiber
J M Sierra-Hernandez, R Rojas-Laguna, E Vargas-Rodriguez et al.
- Low-threshold dual-wavelength erbium-doped fiber laser based on ring core fiber with core-offset structure
Y H Qi, J Sun, W X Jin et al.

This content was downloaded from IP address 139.184.14.159 on 23/09/2017 at 19:55

IOP Publishing | Astro Ltd Laser Physics
Laser Phys. **27** (2017) 105104 (8pp) https://doi.org/10.1088/1555-6611/aa8287

Erbium-doped fiber ring laser with wavelength selective filter based on non-linear photonic crystal fiber Mach–Zehnder interferometer

W A Khaleel[1,2] and A H Al-Janabi[2]

[1] Laser and Optoelectronics Department, College of Engineering, Nahrain University, Baghdad, Iraq
[2] Institute of Laser for Postgraduate Studies, University of Baghdad, Baghdad, Iraq

E-mail: wurooda.khaleek@eng.nahrainuniv.edu.iq and hadi.janabi@ilps.uobaghdad.edu.iq

Received 29 April 2017, revised 27 June 2017
Accepted for publication 13 July 2017
Published 21 September 2017

Abstract

A high output power, stable wavelength spacing and switchable multi-wavelength erbium-doped fiber laser has been demonstrated experimentally using a combination of non-linear photonic crystal fiber Mach–Zehnder (MZI) interferometer with polarization dependent loss effect. This MZI functions together with a polarization controller (PC) as a wave selecting filter (WSF). Adjusting the PC within the WSF part gives rise to three emissions as single, dual and triple wavelengths. Multi-wavelength laser with maximum spacing of 1.6 nm was achieved by controlling the polarization state in a ring cavity. Such stable wavelength spacing aroused interest in wavelength-division-multiplexer systems. Output power around −3 dB at 1550 nm wavelength, with small power fluctuation for each line, was recorded at room temperature. The measured 3-dB laser line-width was 0.03 nm, with a high side-mode suppression ratio of 48 dB.

Keywords: multi-wavelength, erbium-doped ring fiber laser, Mach–Zehnder interferometer, wavelength selective filter

(Some figures may appear in colour only in the online journal)

1. Introduction

Multi-wavelength erbium-doped fiber lasers (EDFLs) have potential applications in many areas of photonics and telecommunications. These fiber laser sources have also been employed in fiber optic testing, fiber sensors, measurement of wavelength division multiplexing (WDM) components, and spectroscopy [1–3]. The requirements of WDM systems are: large number of channels over a large wavelength span; moderated output power (of the order of 100 μW per channel), with power distributed uniformly over channels; stable, fixed wavelength spacing; and small power variation with high side-mode suppression ratio (SMSR) for each individual channel [4, 5]. The main challenge in producing stable multi-wavelength lasing in erbium-doped fiber ring lasers (EDFRL) is the strong mode competition induced by the fact that erbium ions saturate mostly homogeneously at room temperature [4, 6]. The key of successful operation of multi-wavelength EDFRL is the suppression of mode competition. One promising solution to suppress the strong mode competition is by employing a single gain medium in combination with a wavelength selective filter (WSF). Currently, WSF design is realized through various techniques such as Fabry–Perot interferometers [7, 8], fiber Bragg grating in Sagnac loop interferometer [9], and in-fiber Mach–Zehnder interferometers (MZIs) [10–12]. Among these, in-line fiber MZI has many attractive advantages, such as broad wavelength operation range, low insertion loss, insensitivity to environmental changes, robustness, compactness and relatively simple fabrication [13, 14]. The output lasing wavelength depends strongly on optical characteristics of MZI and fiber type [15]. For multi wavelength-EDFL applications, MZI can be implemented in various ways and with

 © 2017 Astro Ltd Printed in the UK

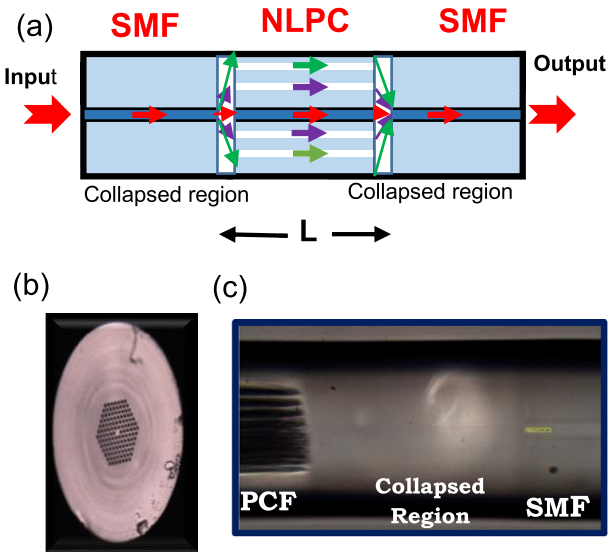

Figure 1. (a) Schematic diagram of the proposed in fiber NLPCF MZI. (b) Microscopic image of the NLPCF cross-section. (c) Microscopic image of the splicing NLPCF/SMF with collapsed region 210 μm.

various types of fibers, for example in the work presented by Lin Ma *et al* [16], in which the MZI was formed by splicing a thinner no-core fiber between two single mode fibers (SMFs). They demonstrated a tunable output laser line with 32 nm tuning range. Dual-wavelength EDFL with tunable wavelength spacing has been achieved using twin core [17], tapered EDF [18] and non-linear photonic crystal fiber (NLPCF) [10]. In [3, 19–21], stable multi-wavelength laser emission was obtained using in-line NLPCF MZI but with variable wavelength spacing. In this paper, a stable multi-wavelength laser operating at around 1550 nm, with constant wavelength spacing, high output power and high SMSR, is demonstrated experimentally using a compact, low loss NLPCF-MZI. Our WSF is based on a combination of SMF-NLPCF-SMF structure with PDL effect. Practically, the WSF is formed by incorporating a short piece of NLPCF in a ring cavity configuration. Optimized splicing parameters were employed to reduce the NLPCF MZI insertion loss and attain high SMSR. The effective refractive index difference between the core mode and cladding modes has been calculated using COMSOL Multiphysics software.

2. In-line NLPCF MZI fabrication and characterization

Figure 1(a) shows the schematic diagram of the proposed in-line NLPCF MZI. This interferometer was implemented by splicing a 7 cm length of NLPCF (SC-5.0-1040 from NKT Photonics Inc.) between two sections of standard SMF (coring SMF-28) using a commercial arc fusion splicer (Fujikura FSM-60S). The NLPCF has cladding formed by six layers of air holes in hexagonal array, with core and cladding diameters of 4.8 μm and 125 μm respectively. Each air hole has a diameter of 1.7 μm and a pitch of 3.3 μm. A microscopic cross-sectional image of the PCF used is shown in figure 1(b). In this type of MZI, the optical characteristics of PCF, such as air hole structure, length of the PCF and the characteristic of splicing structure, are very important parameters. These parameters will decide the spectral response of this WSF [3]. The collapse of air holes in the NLPCF and the mode field mismatching between the NLPCF and the SMF make it not easy to splice them together with good repeatability and low loss. Collapse of air holes in the NLPCF is hard to avoid, but the affected length could be minimized by choosing a weaker fusion arc power and a shorter fusion time. Furthermore, the splicing loss also increases due to the generation of bubbles during the fusion splicing process. The bubble formation comes about due to the softening temperature of the SMF being higher than that of the NLPCF. It is better to introduce a suitable offset, between the inter-fiber contact point and the central axis of electrodes, so the NLPCF is kept away from the center of the discharge zone, and will be less strongly heated. The amount of offset decides the amount of heat being applied to the NLPC; thus, it is almost an easy job to control the region of air hole collapse.

The fabrication of the NLPCF MZI structure is described as follows. First, a short length of NLPCF was cleaved and spliced with cleaved SMF to form the first spliced (collapsed) region. If the NLPCF and the SMF are fusion spliced with automatic mode set in the splicer for splicing SMFs, the length of the air hole collapse region is about a few hundred micrometers, and bubbles are generated. Therefore, manual splicing mode was used with a repeated arc discharge technique, to reduce the splicing loss as much as possible. Secondly, another cleaved end of NLPCF and the end of another SMF were fixed by two holders placed in the splicer.

Then, the input and output ports of the SMF were connected, respectively, to a broadband light source and optical spectrum analyzer, to monitor the interference spectrum. The amount of offset between the fiber contact point and the central axis of electrodes was manually adjusted via the manual mode of splicer until clear fringe visibility was observed. To achieve high visibility with in-line fiber MZI interferometers the two spliced (collapsed) regions need to be identical [22].

Therefore, the fusion splicer was set to the following optimized splicing parameters: −6 bit perfused power, 240 ms perfused time, −22 bit arc one power, 2400 ms arc time, standard arc two power, 2 s arc two power and 10 μm overlap. The length of the collapsed region shown in figure 1(c) is about 210 μm. By applying the above splicing parameters, the insertion loss of NLPCF MZI was reduced to around 11 dB (as depicted in figure 2). 20 dB [19], and 18 dB [15] insertion loss were reported, for the similar in-line PCF MZI.

In the present NLPCF-MZI, the collapsed region allows the input light to split into the core and the cladding of the PCF, resulting in light propagating as core mode and cladding modes respectively. The first collapsed region acts as a beam splitter coupler where the core and cladding modes are excited in PCF simultaneously, while the second collapsed region acts as a beam combiner coupler. The core mode and cladding modes travel along the PCF length (L) with different speeds. Since these modes are characterized by their effective refractive indices (n_{core} and n_{clad}), a relative group delay is developed after the propagation. They (core mode and cladding

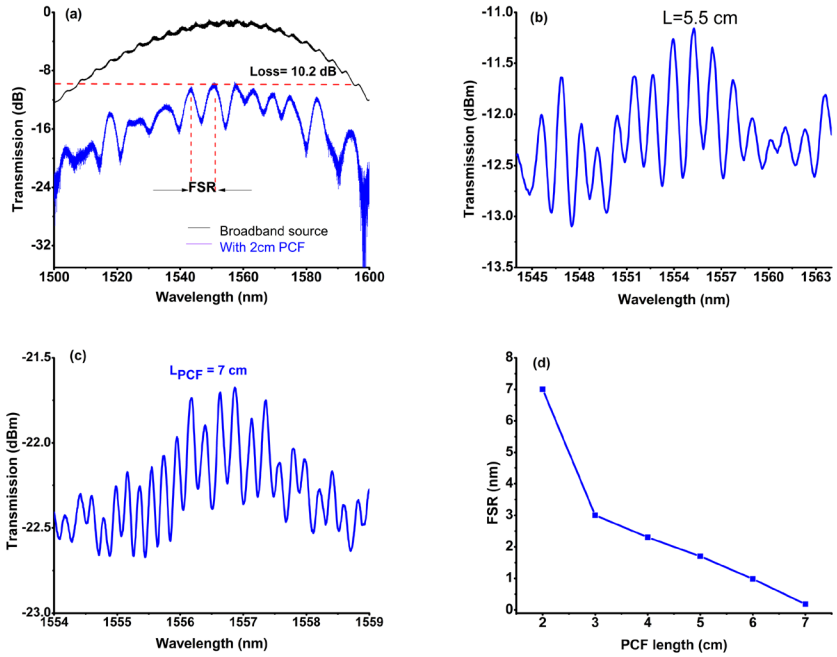

Figure 2. (a)–(c) Transmission spectrum of in-line NLPCF MZI with different NLPCF length: (d) plot FSR as a function of NLPCF length.

modes) recombine at the second collapsed region of the PCF output end. The resulting intensities due to interference of two co-propagating waves can be given as [23]

$$I_{\mathrm{Tot}} = I_1 + I_2 + 2\sqrt{I_1 I_2}\cos(\Delta\varnothing). \tag{1}$$

Here, I_1 and I_2 are the light intensities of core mode and cladding modes at the end of PCF. $\Delta\varnothing$ is the optical phase difference (OPD) between the core mode and the cladding modes, which can be expressed as:

$$\Delta\varnothing = k\Delta n_{\mathrm{eff}} L = \frac{2\pi}{\lambda}\Delta n_{\mathrm{eff}} L. \tag{2}$$

Here, L is the physical length of PCF, Δn_{eff} the difference between the effective refractive indices of the core and cladding, and λ the light wavelength. Equation (2) describes the accumulated OPD along the PCF; the magnitude of this phase difference is mainly dependent on the length of the PCF (L). The interference between the core mode and cladding modes may be constructive, due to the OPD between them. The spacing $\Delta\lambda$ between adjacent constructive peaks (or the free spectral range (FSR)) can be described as:

$$\Delta\lambda = \frac{\lambda^2}{\Delta n_{\mathrm{eff}} L}. \tag{3}$$

The setup of the transmission measurement comprises of a broadband source (SLD1550S-A1 from Thorlabs) and YOKOGAWA AQ6370C optical spectrum analyzer (OSA).

The broadband source was spliced to NLPCF MZI while the other end of the NLPCF MZI was connected to the OSA. The upper part (the black curve) in figure 2(a) represents the broadband source transmission. The transmission spectra of in-fiber PCF MZI with various PCF lengths are illustrated in figures 2(a)–(c). The FSR as a function of the PCF length is shown in figure 2(d). From the results in figure 2, the FSR decreases with increasing PCF length. The FSR is approximately 7 nm at around $\lambda = 1550$ nm for $L = 2$ cm (figure 2(a)). Substituting these values into equation (3), the difference between the effective refractive indices of the PCF core and cladding around 1550 nm comes to be $n_{\mathrm{eff}} = 0.0172$. The mode field distribution and the effective refractive index of core mode and cladding modes were analyzed by the finite element method (FEM; COMSOL Multiphysics 4.2a), as depicted in figure 3. The calculated effective refractive index difference between the core mode and cladding modes comes out to be 0.0174 at 1550 nm (see figure 3(f); the effective refractive indices for the cladding modes are very close to each other, and the lowest loss one has been considered in calculation), which is well matched with the measured value. This confirms that the interference pattern is generated as a result of the OPD between the core mode and the cladding modes propagating along the PCF.

3. Experimental setup

The EDFL with WSF was designed and constructed with a standard ring cavity configuration, as shown in figure 4. A standard ring cavity fiber laser comprises an active gain medium and various related fiber coupled optical components. These optical components include wavelength division multiplexer (WDM), optical isolator, fused coupler, polarization controller and optical pump source. The length of the EDF and out-coupling efficiency of the fiber coupler play a significant role in the performance of an EDFRL. Theoretical calculations (based on theoretical model presented in [24]) have been carried out to select the optimum values of these parameters.

An EDF (EDFC-980-HP from Nufern) with doping concentration of 270 ppm and peak absorption of 7 dB m^{-1} at 975 nm was used as an active gain medium. The EDF has a core numerical aperture of 0.23 and mode field diameter of

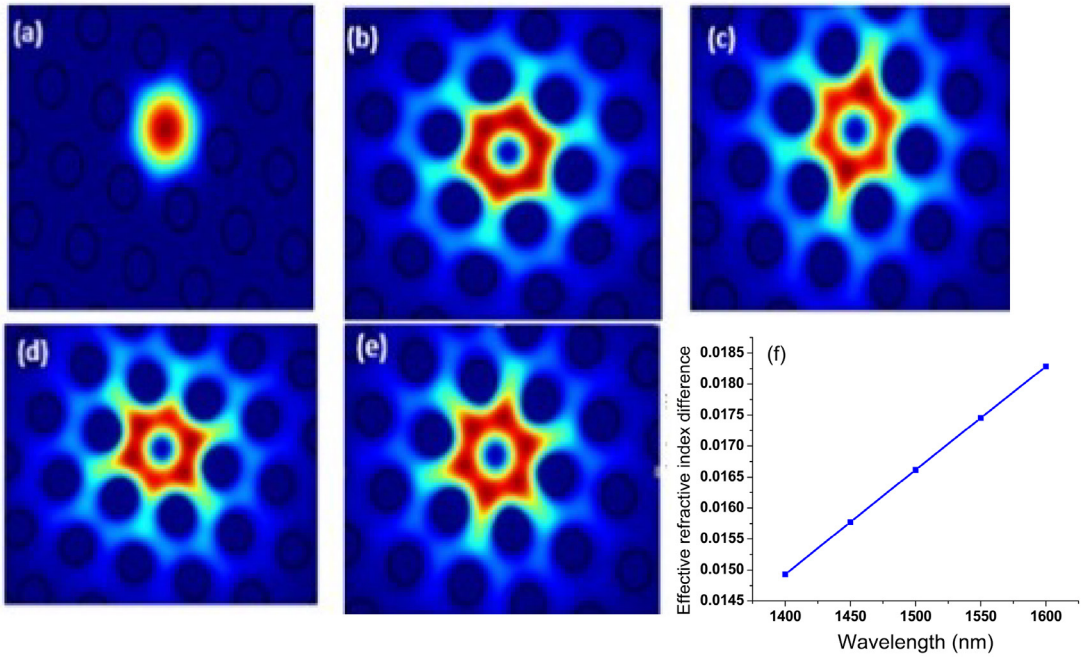

Figure 3. (a) Transverse mode field intensity distribution of core mode. (b)–(e) The mode field distribution of cladding modes. (f) Numerical simulation of relation between the effective refractive index difference (Δn_{eff}) and the operating wavelength.

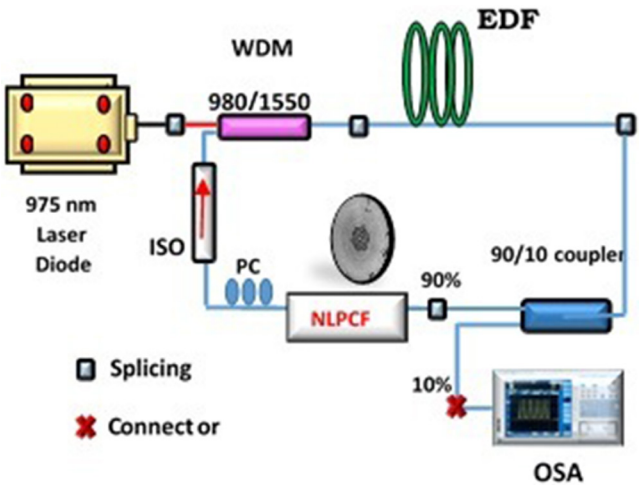

Figure 4. Experimental setup of SMW-EDFL.

5.8 μm at 1550 nm. The EDF was pumped by a 975 nm fiber coupled laser diode (PL980P330J from Thorlabs) with 300 mW maximum output power. The pump light was coupled into the ring cavity using a 980/1550 WDM. One end of the EDF was fusion spliced to the output port of the WDM, while the other end was fusion spliced to the input port of a 10:90 fiber output coupler. The laser output was led out from the cavity by a 10:90 fiber output coupler. An OSA with 0.02 nm resolution was connected through the 10% arm of 10:90 fiber coupler to monitor output spectrum. To increase the OPD between the core mode and cladding modes, a 7 cm length of NLPCF (SC-5-1040, NKT Photonics) was spliced through the 90% feedback arm of 10:90 fiber coupler. An optical isolator was employed to ensure unidirectional light propagation. Finally, WSF is formed by the in-line NLPCF MZI combined with the PC. This filter has an insertion loss of nearly 11 dB (see figure 2(c)).

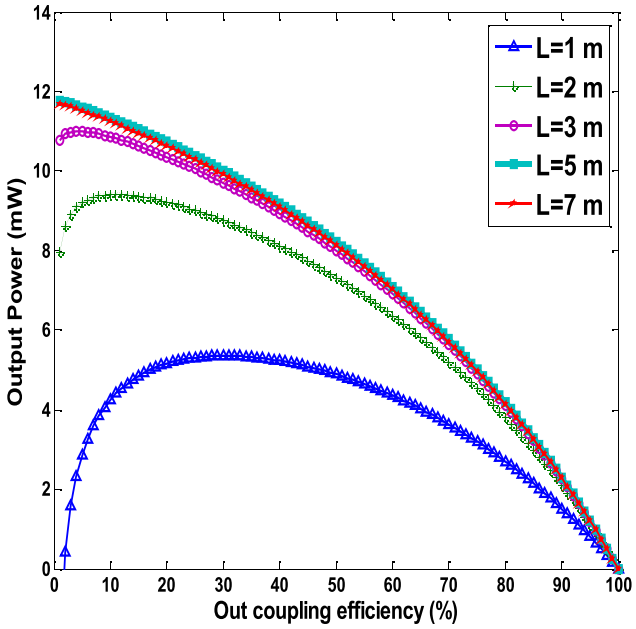

Figure 5. Calculated laser output power versus different out coupling efficiency. EDF has a peak absorption of 7 dB m^{-1} at 975 nm. The input pump power is 150 mW.

4. Results and discussion

Firstly, continuous wave (CW) EDFRL has been designed and constructed experimentally before inserting the WSF. Figure 5 shows the calculated variation of laser output power versus out coupling efficiency for various EDF lengths. From this figure, it is clear that for $L \geqslant 2$ m the laser oscillates at all values of coupling efficiency, and maximum output power occurs for out coupling efficiency $\leqslant$10%.

The output laser power increases gradually with the out coupling efficiency until the out-coupling efficiency reaches

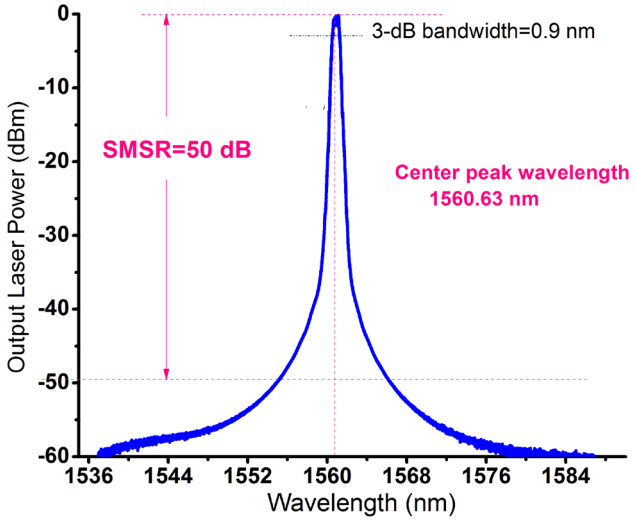

Figure 6. Measured laser output spectrum of EDFRL without WSF.

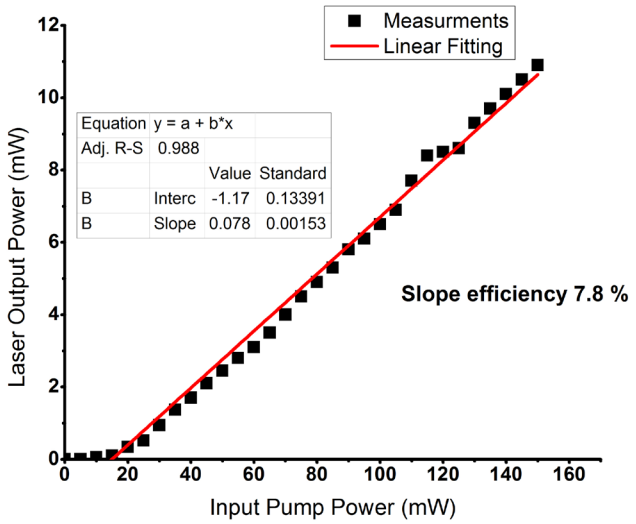

Figure 7. Measured laser output spectrum versus the input pump power of EDFRL without WSF.

about 10%. At this value, the laser power reaches a maximum, and then decreases, due to the loss, even when the EDF length is increased. A 5 m EDF length has been used as the optimum length for an active gain medium (see figure 5, where the maximum output power occurs at this EDF gain medium length).

The peak laser wavelength and the 3 dB linewidth of lasing spectrum occur at 1560.63 nm and 0.9 nm respectively for EDFRL without WSF, as shown in figure 6. The threshold pumping power is 18.5 mW, and the maximum output power 10.9 mW at input pumping power of 150 mW. The relationship between the input pump power and laser output power was measured as shown in figure 7. The laser slope efficiency was 7.8%.

In a ring cavity without WSF or PC, due to the strong mode competition induced by the homogeneous broadening of EDF, different wavelengths with almost identical polarization states will be travelling through the ring cavity [12]. The lasing wavelength represents the fundamental mode propagating through the ring cavity. When a short piece of NLPCF is incorporated into the ring cavity, this fundamental mode and other high order modes will be excited, and will interfere with each other along the NLPCF. These interference patterns will be recoupled into a fundamental mode along the second collapsed region but with spectral shifting. This shift in lasing wavelength depends mainly on the state of polarization (SOP) of the incident light entering the PCF. In general, WSF based on PDL is potentially effective when it is combined with PC. Because the lasing wavelength of the PCF MZI and the peak refractive-index modulation are entirely dependent on the SOP of the incident light into the PCF, birefringence varies the MZI transmission characteristics. To compensate the loss and gain of the lasing wavelength, the PC is adjusted to rotate the SOP to maintain continuous adjustment of the birefringence within the ring cavity [10]. Therefore, the PC with WSF acts as a spectrally selecting element, which should be employed to limit the number of modes over which the laser may effectively oscillate. Hence, the adjustment of the PC will rotate the polarization state entering the fiber ring cavity, and enable spectral discrimination.

By adjusting the PC for a certain angle, a typical single-wavelength laser output was obtained, as shown in figure 8(a) (solid line). The laser output was operated around 1550 nm with output power of −4 dBm. This is the highest output power obtained in comparison with previously published work [11, 15, 19]. By finely adjusting the PC, the polarization state entering the fiber ring cavity will be red shifted (dash line). This single laser emission was shifted from 1549.7 nm to 1552.05 nm. The measured 3 dB linewidth of the laser was less than 0.03 nm, with SMSR of about 56 dB (as depicted in figure 8(a)). Compared with reported published work [11, 15, 21], this is the highest SMSR. The displayed OSA spectrum for the laser operation at room temperature for 1 h indicates a stable and clean operation (see figure 8(b)) with a very small wavelength shift of about ±0.01 nm, and peak power fluctuations of the peak wavelength (1549.7 nm) measured to be around 0.225 dB (as shown in figure 8(c)). By further adjusting the PC, a typical dual-wavelength laser was produced, as shown in figure 9(a) with a spacing of 1.4 nm between the dual peak wavelengths of 1549.3 nm and 1550.7 nm. Similarly, these two lines could be shifted with constant wavelength spacing by finely adjusting the PC (see figure 9(a)). Repeated recording of dual-wavelength spectra over a period of 1 h showed reproducible results, as shown in figure 9(b).

For the dual wavelength lasing case, the SMSR was 56 dBm. The wavelength shift was less than 0.02 nm, and the peak power fluctuations of the wavelengths 1549.3 and 1550.7 nm were 0.288 dB and 1 dB respectively (figure 9(c)). The PC was readjusted until triple-wavelength laser appeared. Figure 10(a) illustrates the measured spectral emission at 1548.9, 1550.6 and 1552.2 nm and maximum output power −1 dB. The combination of WSF and PC gives the ability to tune these lines, producing fixed spectral separations. This constant or fixed wavelength spacing indicates a comb-like behavior, unlike previously reported works [3, 19, 21] in which these three lines can be tuned, which produced varying spectral separation and low peak output power. The spectral response of the laser was recorded every 10 min for a duration of 1 h, to ensure its stability (figure 10(b)). Triple-wavelength

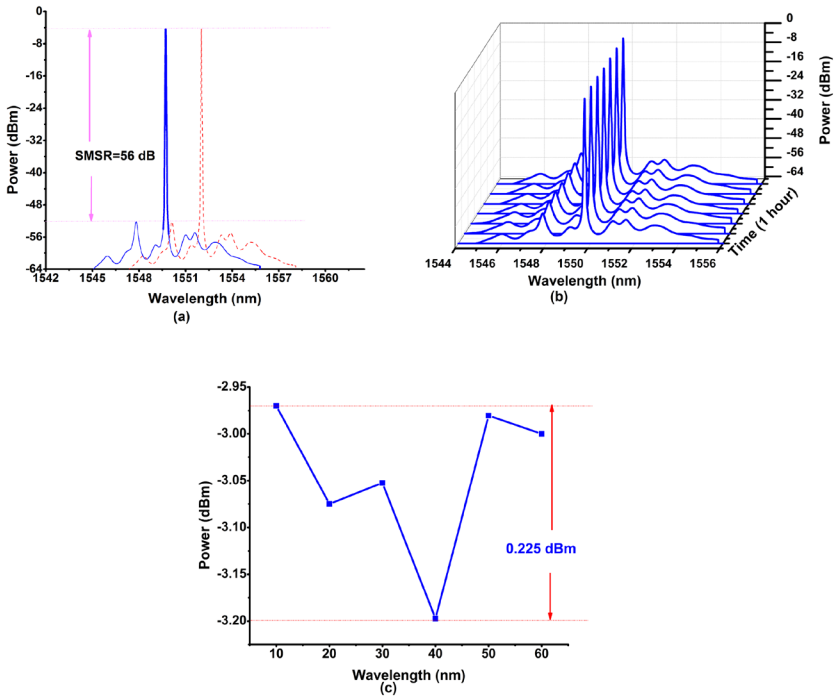

Figure 8. (a) Shifting of single-laser output spectrum. (b) Measured output laser spectrum recorded every 10 min and (c) measured laser peak power fluctuation.

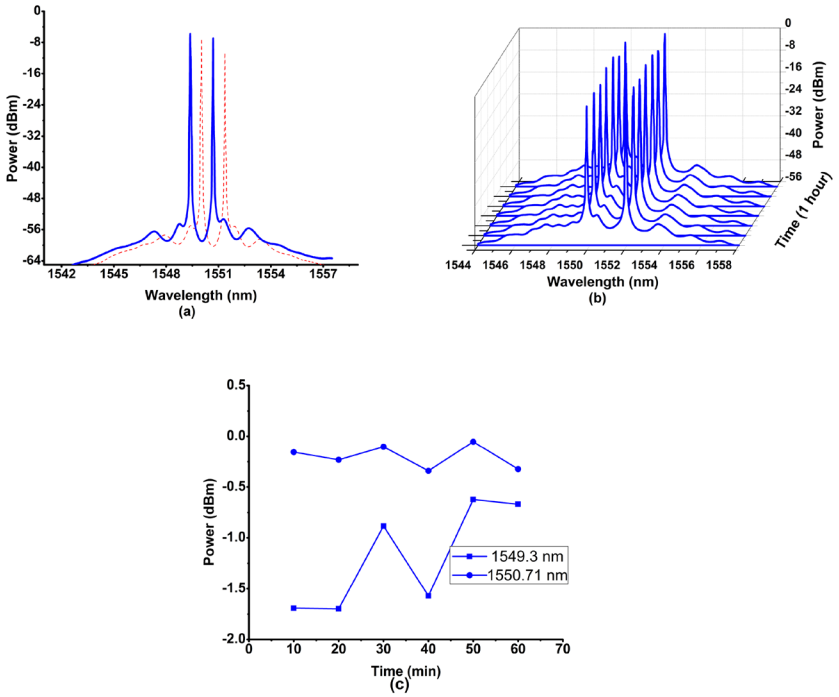

Figure 9. (a) Shifting of dual-laser output spectrum. (b) Measured output laser spectrum recorded every 10 min and (c) measured laser peak power fluctuation.

emission shows a remarkable stability, with 48 dB SMSR. These interesting features are due to low loss and to identical collapsed regions between NLPCF and standard SMF, through improvement of the splicing fusion process. Moreover, the measured peak power variations were 2.33 dB, 3.53 dB, and 2.6 dB for the wavelengths 1548.9, 1550.6 and 1552.2 nm respectively (figure 10(c)). All experimental work was carried out at room temperature.

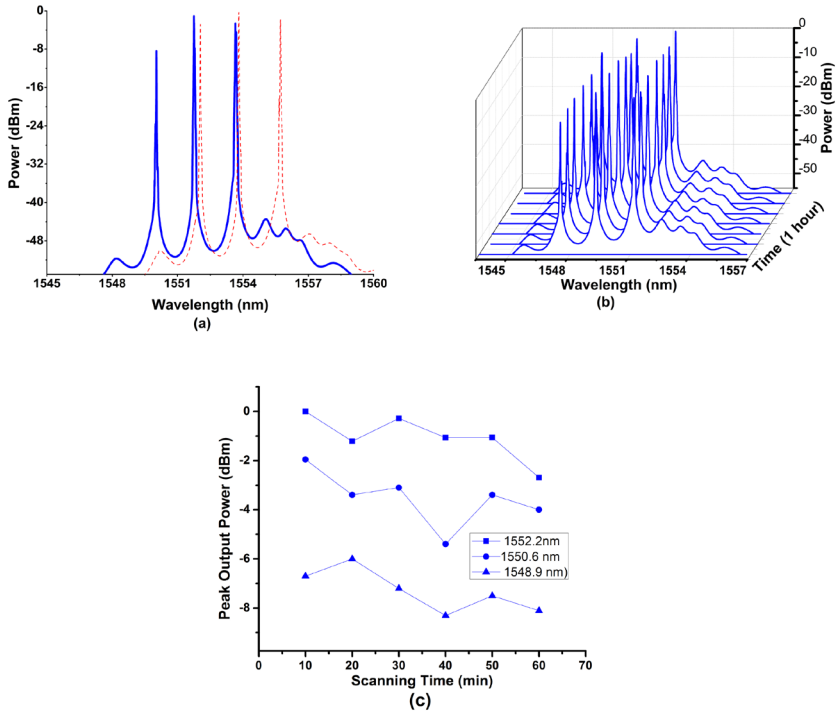

Figure 10. (a) Shifting of triple-laser output spectrum. (b) Measured output laser spectrum recorded every 10 min and (c) measured laser peak power fluctuation.

5. Conclusions

High output power with fixed (~1.6 nm) wavelength spacing has been demonstrated experimentally for the first time by designing and constructing an EDFL with WSF. The NLPCF-MZI with the PC acts as a WSF and was implemented by splicing 7 cm of NLPCF between two segments of SMF. When the optimized splicing parameters were employed, the splice loss between the nonlinear PCF and the SMF was reduced to around 1 dB for each splicing region, and the PCF MZI insertion loss was about 11 dB. A difference of 0.0174 in effective refractive indices between the PCF's core and cladding modes was calculated using COMSOL software, which is well matched with the measured values. Incorporating the WSF inside the EDFL gives access to single-, dual- or triple- wavelength emission with high output power, and fixed wavelength separation by adjusting the PC. The measured peak power for single laser emission at 1549.7 nm was about −4 dBm with 0.225 dB peak power fluctuation over a period of 1 h. For the dual lasing case, the emitted wavelength had 56 dB SMSR, and 1.6 nm constant wavelength separation and high output power around −1 dBm. Moreover, a very stable triple-wavelength emission located at 1548.9 nm, 1550.6 nm and 1552.2 nm, with maximum peak power variation of 2.33 dB, 3.53 dB and 2.6 dB respectively, has been produced; these wavelengths having 1.6 nm wavelength separation and a high SMSR of 48 dB.

Acknowledgments

This work was partially supported by the Institute of Laser for Postgraduate Studies (ILPS), University of Baghdad (UOB).

References

[1] Feng X, Tam H Y and Wai P K A 2006 Switchable multiwavelength erbium-doped fiber laser with a multimode fiber Bragg grating and photonic crystal fiber *IEEE Photonics Technol. Lett.* **18** 1088–90
[2] Zhang Q, Zeng X, Pang F, Wang M and Wang T 2012 Switchable multi-wavelength fiber laser by using a compact in-fiber Mach–Zehnder interferometer *J. Opt.* **14** 045403
[3] Sierra-Hernandez J M, Rojas-Laguna R, Vargas-Rodriguez E, Estudillo-Ayala J M, Mata-Chavez R I, Jauregui-Vazquez D, Hemandez-Garcia J C, Andrade-Lucio A and Gutierrez-Gutierrez J 2013 A tunable multi-wavelength laser based on a Mach–Zehnder interferometer with photonic crystal fiber *Laser Phys.* **23** 055105
[4] Ana R, Herrera P and Amo M 2013 Multi-wavelength fiber lasers *Current Developments in Optical Fiber Technology* (Rijeka: InTech) ch 17 (https://doi.org/10.5772/53398)
[5] Zhang A, Liu H, Demokan M S and Tam H Y 2005 Fiber ring laser incorporating a highly nonlinear photonic crystal fiber *IEEE Photonics Technol. Lett.* **17** 2535–7
[6] Wang F 2015 Research of multi-wavelength fiber laser mode competition suppression technology *Proc. SPIE* **9795** 97953M–9
[7] He W, Zhu L, Dong M and Luo F 2016 Multi-wavelength tunable erbium-doped fiber laser based on Fabry–Perot filter and Mach–Zehnder interferometer *Microw. Opt. Technol. Lett.* **58** 1790–4
[8] Pan S, Lou C and Gao Y 2006 Multi-wavelength erbium-doped fiber laser based on inhomogeneous loss mechanism by using of a highly nonlinear fiber and a Fabry–Perot filter *Opt. Express* **13** 1113–8
[9] Feng S, Xu O, Lu S, Ning T and Jian S 2008 Switchable multi-wavelength erbium-doped fiber ring laser based on cascaded polarization maintaining fiber Brag grating in Sangnac loop interferometer *Opt. Commun.* **281** 6006–10
[10] Ahmad H, Soltanian M R K, Pua C H, Zulkifli M Z and Harun S W 2013 Narrow spacing dual-wavelength fiber

laser based on polarization dependent loss control *IEEE Photonics J.* **5** 1502706
[11] Chen W, Lou S, Wang L, Zou H, Lu W and Jian S 2012 Switchable multi-wavelength fiber ring laser using a side-leakage photonic crystal fiber based filter *Opt. Laser Technol.* **44** 611–6
[12] Ahmad H, Soltanian M, Alimadad M and Harun S W 2014 Stable narrow spacing dual-wavelength Q-switched graphene oxide embedded in a photonic crystal fiber *Laser Phys.* **24** 105101
[13] Lee B, Kim Y, Park K, Eom J, Kim M, Rho B and Choi H 2012 Interferometric fiber optic sensors *Sensors* **12** 2467–86
[14] Wang Q, Kong L, Dang Y, Xia F, Zhang Y, Zhao Y, Hu H and Li J 2016 High sensitivity refractive index sensor based on splicing points tapered SMF-PCF-SMF structure Mach–Zehnder mode interferometer *Sensors Actuators* B **225** 213–20
[15] Sierra-Hernandez J M, Rojas-Laguna R, Vargas-Rodriguez E, Estudillo-Ayala J M, Jauregui-Vazquez D, Guzman Chavez A D and Zaca-Moran P 2013 A tunable multi-wavelength erbium-doped fiber laser based on a Mach–Zehnder interferometer and photonic crystal fiber *Laser Phys.* **23** 125103
[16] Man L, Qi Y, Kang Z, Bai Y and Jian S 2014 Tunable fiber laser based on the refractive index characteristic of MMI effects *Opt. Laser Technol.* **57** 96–9
[17] Yin G, Lou S, Wang X and Han B 2014 Dual-wavelength erbium-doped fiber laser with tunable wavelength spacing using twin core fiber-based filter *J. Opt.* **16** 055404
[18] Ali M, Ibrahim S A, Abu Baka M H, Noor A S, Ahmad S B, Zamzuri A K and Mahd M A 2014 Tapered-EDF-based Mach–Zehnder interferometer for dual-wavelength fiber laser *IEEE Photonics J.* **6** 5501209
[19] Chen W, Lou S, Wang L, Li H, Guo T and Jian S 2009 Switchable multi-wavelength fiber ring laser based on a compact in-fiber Mach–Zehnder interferometer with photonic crystal fiber *Laser Phys.* **19** 2115–9
[20] Zheng W, Ruan S, Zhang M, Liu W, Zhang Y and Yang X 2013 Switchable multi-wavelength erbium-doped photonic crystal fiber laser based on nonlinear polarization rotation *Opt. Laser Technol.* **50** 145–9
[21] Gomez R, Sanchez G, Rios A, Pensado M, Uribe J, Aguilar R, Anzueto J and Ramirez V 2015 Multi-wavelength switching of an erbium-doped fiber ring laser based on the cross-sensitivities features of tapered fiber filters *Opt. Rev.* **22** 526–31
[22] Cárdenas-Sevilla G A, Finazzi V, Villatoro J and Pruneri V 2011 Photonic crystal fiber sensor array based on modes overlapping *Opt. Express* **19** 7596–602
[23] Du J, Dai Y, Lei G, Tong W and Shu C 2010 Photonic crystal fiber based Mach–Zehnder interferometer for DPSK signal demodulation *Opt. Express* **18** 7917–22
[24] Barnard C, Myslinski P, Chrostowski J and Kavehrad M 1994 Analytical model for rare earth-doped fiber amplifiers and lasers *IEEE J. Quantum Electron.* **30** 1817–30